THESIS

DEPOSITION OF STRONTIUM-90 IN SOIL AND VEGETATION AT VARIOUS LOCATIONS SURROUNDING THE FUKUSHIMA DAIICHI NUCLEAR POWER PLANT

Submitted by

Joseph E. Ball

Department of Environmental and Radiological Health Sciences

In partial fulfillment of the requirements

For the Degree of Master of Science

Colorado State University

Fort Collins, Colorado

Fall 2015

Master's Committee:

Advisor: Georg Steinhauser

Alexander Brandl
Robert Gundmestad

ABSTRACT

DEPOSITION OF STRONTIUM-90 IN SOIL AND VEGETATION AT VARIOUS LOCATIONS SURROUNDING THE FUKUSHIMA DAIICHI NUCLEAR POWER PLANT

As a result of the 2011 Honshu earthquake, a tsunami formed off the coast of Japan that overtook the Fukushima Daiichi Nuclear Power Plant (FDNPP). This tsunami caused a cooling system failure at FDNPP. Due to this failure, a meltdown and subsequent release of radioactivity occurred.

This project attempts to determine if ^{90}Sr was released during the meltdown and could be detected in the surrounding environment. Vegetation and soil samples were collected from eight locations near the FDNPP ranging from 0 km to 40 km. The samples were subjected to a radiochemical separation to isolate ^{90}Sr from other potential radionuclides in the samples. This was done to eliminate interference from those radionuclides in our analysis of ^{90}Sr in the Hidex 300SL liquid scintillation counter (LSC).

Results of the analysis determined with 95% confidence that ^{90}Sr was detectable in both vegetation and soil samples within 4.1 km of the FDNPP. The highest levels of ^{90}Sr activity concentration fall in-between the activity concentrations of naturally-occurring radionuclides in the earth's upper crust and do not pose a significant health threat to humans due to ingestion.

ACKNOWLEDGMENTS

This project would not have been possible without the guidance of Dr. Georg Steinhauser. His guidance kept this analysis focused and prevented mission creep in addition to providing hands-on expertise in the radio-analytical laboratory. I would also like to thank my committee members as a whole for their support and unique perspective through this program.

Dr. Thomas Johnson and Dr. Alexander Brandl provided exceptional technical support for the software programs used with the detectors employed in this study. Their knowledge enabled rapid screening for low-activity samples.

I would like to thank the many members of the College of Veterinary Medicine and Biomedical Sciences who made possible the numerous educational experiences I have had while attending Colorado State University. These experiences include formal lectures, informal discussions, and a tour of the Los Alamos National Laboratory.

The Central Rocky Mountain Chapter of the Health Physics Society provided many exposures to operational health physics and valuable insight into the effect of this analysis.

Dr. Katsumi Shozugawa is the driving force behind this project. Without him, samples for this analysis would not have been available.

TABLE OF CONTENTS

LIST OF TABLES

LIST OF FIGURES

INTRODUCTION

Background

On March 11, 2011 at 14:46 (local time), an earthquake measuring a magnitude of 9.0 occurred with its epicenter in the Pacific Ocean approximately 130 km east of Sendai (Japan) and 163 km northeast of the Fukushima Daiichi Nuclear Power Plant (FDNPP). (Thielen, 2012) This caused a devastating tsunami that reached heights of up to 40.5 m.

The FDNPP was operated by the Tokyo Electric Power Company (TEPCO). The FDNPP consists of six reactors utilizing the boiling water reactor design. (Schwantes, 2012 Volume 46) These reactors were commissioned between 1971 and 1979 and were protected by a 10 m seawall (Lipscy, 2013). Unfortunately, the tsunami reached a height of 14 m at the plant site. The tsunami hit the FDNPP at approximately 15:38 and damaged the water intake buildings. It also destroyed the diesel generators that are used for emergency power generation. These two events relegated the main cooling system of the plant inoperable. (Thielen, 2012) Luckily, the reactors that were in operation at the time of the earthquake (units 1, 2 and 3) were automatically shut down prior to the tsunami due to the seismic signals generated by the earthquake.

Although the nuclear reaction was stopped, the decay heat of fission products in the reactor was approximately 20 MW. (Steinhauser G. B., 2014) This heat caused damage and partial meltdown of the fuel elements. (Steinhauser G. S., 2013) Core material started melting at 1500 K, but the temperature of the core remained below 2670 K. (Kirchner, 2012) This is important because “refractory elements were mobilized only to a minor extent” (Steinhauser G. B., 2014)

As a result of the accident at the FDNPP, many volatile radionuclides such as ^{131}I, ^{134}Cs, and ^{137}Cs were released and subsequently detected (Steinhauser G. B., 2014). Not much effort has been given to determining the content of ^{90}Sr surrounding the FDNPP as it is time-consuming, laborious, and is suspected to have been mostly retained in the reactor instead of venting to the atmosphere. (Schwantes, 2012 Volume 46) This project is important because ^{90}Sr is known as a bone-seeker in humans due to its chemical similarity to calcium and may cause leukemia and skeletal cancer. (Steinhauser G. S., 2013)

Following a nuclear event, such as a nuclear explosion or the meltdown of a core at a nuclear power plant, there is a wide spectrum of radionuclides released. Many of them are easily quantified and reported to the public (e.g., $^{134,137}Cs$, ^{131}I) due to their emission of characteristic gamma radiation (photons). Those radionuclides that emit photons can be identified using a gamma detector such as a thallium-doped sodium iodide (NaI(Tl)) or a high-purity germanium (HPGe) detector. Identification occurs within seconds to minutes using these detectors based on variables such as sample activity or detector efficiency. Gamma emission takes the form of at least one discrete energy. These emissions are unique to the radionuclide in question. This is useful in the identification of unknown gamma-emitting radionuclides as each has a unique gamma emission spectrum. See Figure 1: NaI(Tl) Spectrum for Cobalt-60 for an example. Notice the discrete energy counts at 1174 and 1332 keV.

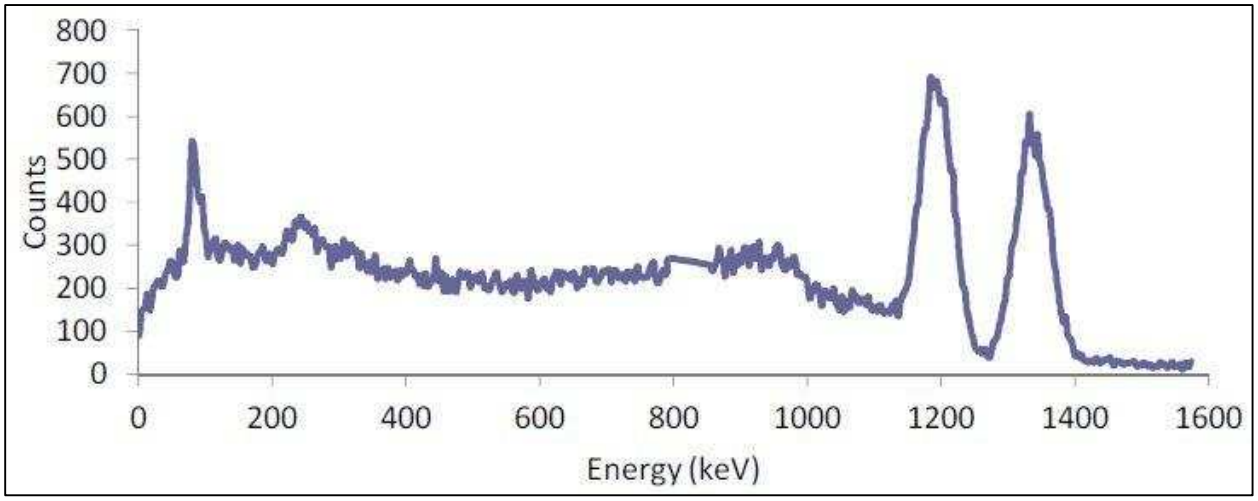

Figure 1: NaI(Tl) Spectrum for Cobalt-60

Some radionuclides are much more difficult to identify, as they do not emit gamma photons. This is true in the case of ^{90}Sr, which emits only beta radiation (β^-). In simple terms, beta decay occurs when a nucleus contains too many neutrons for stability and decays in an effort to achieve nuclear stability. This decay involves an excess neutron that changes into a proton, electron and anti-neutrino. The proton remains in the nucleus, but the electron and anti-neutrino are ejected from the nucleus. The energy released when the neutron changes into a proton is distributed among the emitted electron, emitted anti-neutrino, and recoil energy to the originating nucleus. This distribution of energy is the reason the ejected electron does not display a discrete energy as in gamma radiation.

The beta energies are unique to a radionuclide but are different from gamma energies in that they display a continuous range of energies instead of one or more discrete energies. The fact that the beta energies display a continuous energy distribution instead of a discrete energy distribution makes identification much more difficult than gamma emissions. See Figure 2: Liquid Scintillation Detection Curves for an example of the continuous energy distribution of two separate beta-emitting radionuclides.

In this figure, two individual beta-emitting radionuclides are shown in separate sample analyses. If both of these radionuclides were part of the same sample analysis, the curves would be combined. If this was the case, the curves would overlap and the energy of one radionuclide would be indistinguishable from the other. This is why separation of radionuclides prior to identification of an unknown radionuclide is the method of choice.

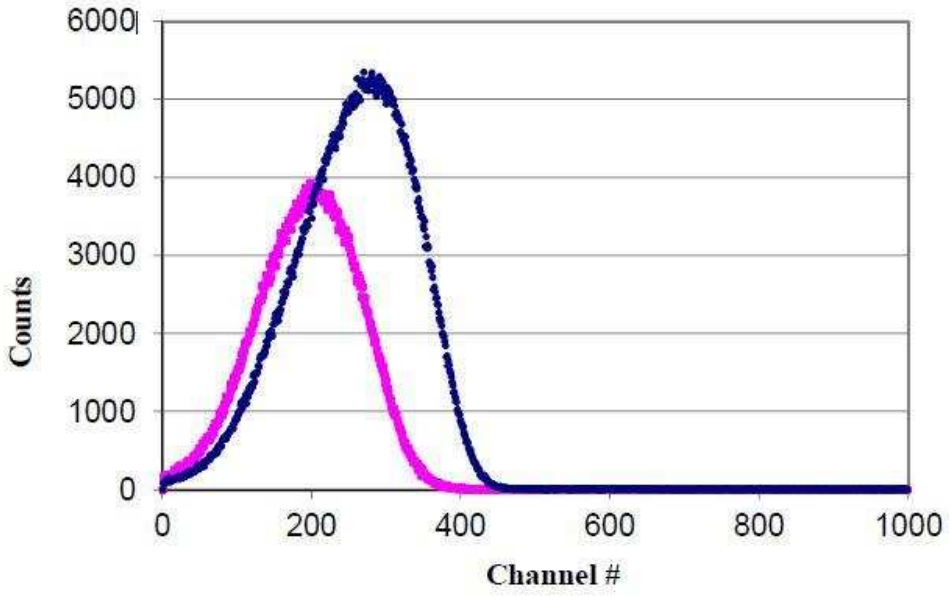

Figure 2: Liquid Scintillation Detection Curves

The instrument of choice for detecting low-level beta radiation is the liquid scintillation counter (LSC). Originally developed to identify low-levels of tritium in water, the LSC works by electro-chemical stimulation of a cocktail in which the radionuclide is placed.

Fission and Neutron Activation

Fission

Neutron capture may result in fission of heavier atoms. For neutron capture to occur, the captured neutron must be a thermal neutron. Thermal neutrons are neutrons that have the same kinetic energy distribution as gas molecules in their environment and usually have a most probable energy of 0.025 eV. (Cember & Johnson, 2009) Whenever a thermal neutron is

captured and creates fission, it is considered thermal fission. Fission can occur as a result of interaction with higher energy neutrons, but the probability decreases as the neutron energy increases. The probability of fission is referred to as the cross section for fission σ_f. Fission most commonly results in the production of two fission products (ternary fission products, such as tritium, are also possible), kinetic energy, neutrons, and gamma rays. For ^{235}U, 2.5 neutrons on average are released per thermal fission with a total energy release of approximately 200 MeV. These fast neutrons then can either induce further fissions or can be captured after moderation to create activation products (Cember & Johnson, 2009).

Fission products are produced with yields approximated by the curve in Figure 3: Fission Product Yield. The most probable fission products have atomic masses in the 90-100 amu and 130-145 amu ranges. Since these products tend to be neutron-rich, they decay via beta decay to achieve nuclear stability. Usually, the half-lives of fission products are short (seconds to hours). ^{90}Sr is one of the longer-lived fission products ($T_{1/2}$ = 28.79 yrs) and is produced via thermal neutron fission of ^{235}U with a probability of 5.73% (Magill, 2012)

^{90}Sr (atomic mass of 90 amu) is a fission product with one of the higher rates of occurrence. Once formed, ^{90}Sr decays via beta emission 100% of the time with a maximum energy ($E_{\beta,max}$) of 546 keV.

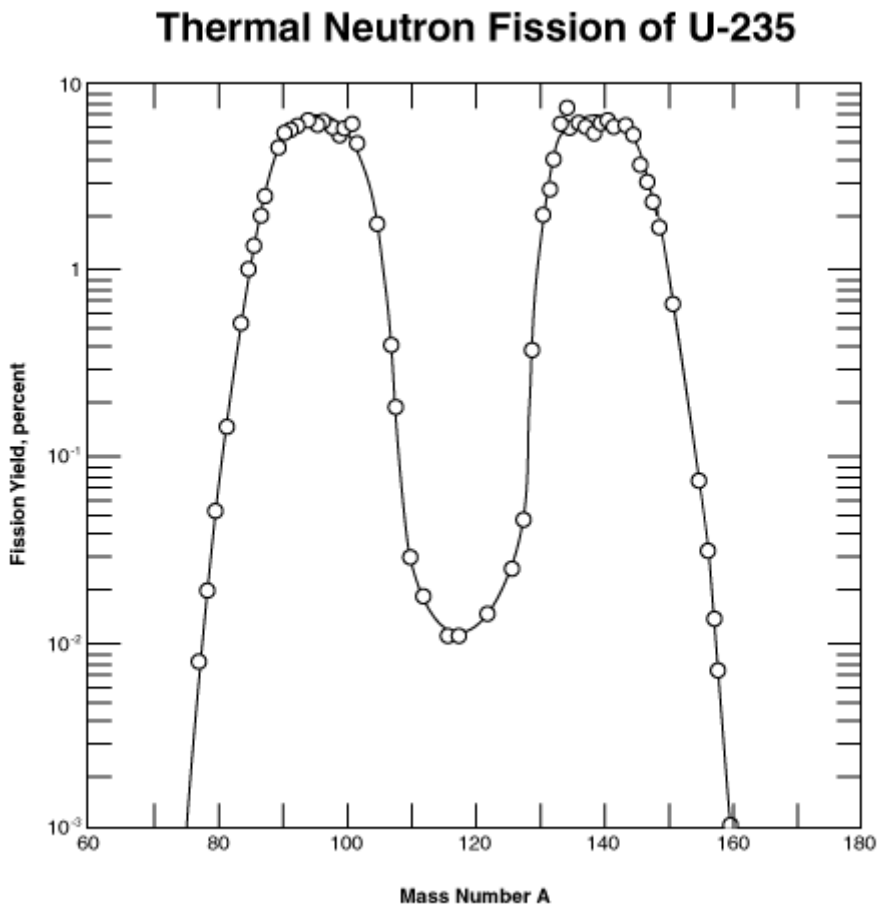

Figure 3: Fission Product Yield (Nuclear Fission Yield)

Neutron Activation

Neutron activation can also occur instead of fission when a thermal neutron is captured by an atomic nucleus. The activation of the nucleus sometimes results in instability. This instability is known as radioactivity and gives rise to some form of radioactive decay.

The activity (*A)* of a radionuclide as a result of neutron activation is dependent on several variables. First of these is the amount of atoms of the nuclide (*N*) being irradiated. Second is the cross section (σ) for thermal neutron capture. Another variable is the neutron flux rate ($\dot{\varphi}$) to which the nuclide is exposed, which is the amount of thermal neutrons available for capture.

Finally, the length of time the sample is irradiated, and the decay constant (λ) are the last two variables. The decay constant is defined as:

$$\lambda = \frac{\ln(2)}{T_{1/2}} \quad (1)$$

where $T_{1/2}$ is the physical half-life of the activation product

It is necessary to consider the matrix surrounding the sample, since that can also influence the neutron flux rate. Assuming an unshielded flux rate within the sample, the equation used to calculate the activity following neutron irradiation is: (Cember & Johnson, 2009)

$$A(t) = N\sigma\dot{\varphi}\left(1 - e^{-\lambda t_{irr}}\right) \quad (2)$$

where:

λ = decay constant of the nuclide produced (s^{-1})

N = number of target atoms being irradiated

σ = cross section for neutron activation (cm^2)

$\dot{\varphi}$ = neutron flux rate (neutrons cm^{-2} s^{-1})

t_{irr} = irradiation time of sample (s)

In order for ^{90}Sr to form via neutron activation, ^{88}Sr would need to capture a thermal neutron to form ^{89}Sr. Then ^{89}Sr would need to capture a thermal neutron as well. Due to the small cross-sections of ^{88}Sr and ^{89}Sr, ^{90}Sr formation due to neutron activation is highly unlikely. The cross-sections for neutron capture in ^{88}Sr and ^{89}Sr are 0.0058 b and 0.42 b respectively as compared to ^{238}U with a cross-section of 4,198 b, which undergoes neutron activation much more frequently. Therefore, in a nuclear reactor, ^{90}Sr is much more easily formed via fission than neutron activation.

Liquid Scintillation Counting

Similar to the other types of scintillation detectors, liquid scintillation counters are comprised of two parts: a scintillator and a photomultiplier tube (PM). A scintillation cocktail contains scintillator compounds and an organic solvent. When using liquid scintillation detectors, the sample is added directly to the scintillation cocktail. This allows for a better efficiency of detection for low-energy betas and alpha particles because there is no attenuation by air or detector window. (Ball, 2014)

When an energized particle (beta) is released from the sample, its energy is transferred primarily to a solvent molecule. This energy excites the solvent molecule ground-state electrons into a higher energy state. The energy from this excited-state solvent molecule is then transferred to another solvent molecule. This process continues until the energy from a solvent molecule is transferred to a scintillator molecule. Once transferred to a scintillator molecule, the energy is released in the form of multiple, visible light photons (prompt fluorescence). This occurs as the excited scintillator electrons de-excite and fall to their ground state. The visible light photons then travel toward the photomultiplier tube where they are converted to an electronic signal. (Ball, 2014) Each beta that interacts with the scintillator liquid causes multiple photon releases. The LSC detects these photons and uses a very small time window to denote the multitude of photons as a count. In this fashion, one beta interaction correlates with one count of the detector. These counts can be divided by the length of time the sample is measured to get a count rate (usually expressed in counts per second (cps) or counts per minute (cpm)).

Liquid scintillation detectors depend on the transmission of light to produce a signal. For this reason, if light cannot escape the medium, no signals can be produced. There are two common circumstances in which light transmittance is reduced. (Ball, 2014) The first of these is if the sample is colored. This coloring affects the transmittance of visible light to the detector

and is known as color quench The second of these is if the sample contains chemicals that absorb the transmitted energy before it reaches a scintillator molecule, thereby reducing the amount of light transmitted to the detector. This is known as chemical quench. Quench in either form, color quench or chemical quench, lowers the energy range and number of events observed by the detector.

The samples in the Hidex 300SL liquid scintillation detector are surrounded by three photomultiplier tubes. This positioning of three PM tubes is an attempt to optimize the sample signals produced by tracking coincidence events among the PM tubes. Coincidence events are characterized as events occurring within a defined coincidence interval (typically a very short period of time). Coincidence events can be used to discard counts not likely produced by the sample or to identify the presence of quench. If a single event is seen in one of the three PM tubes, it is likely due to background such as cosmic radiation. A ratio can be created of events seen in all three PM tubes to events seen in two PM tubes. Events may potentially be seen only in two tubes due to color in the sample or chemicals that absorb energy. This ratio is termed the Triple to Double Coincidence Ratio (TDCR) and can be used to determine quench within the sample.

One disadvantage of the liquid scintillation detector is that liquid inherently must be contained. Depending on the material of the container, light photons can either be emitted or absorbed. Glass is the most common container material because it is transparent. However, glass naturally contains potassium (K) and therefore ^{40}K. ^{40}K can emit additional beta particles into the cocktail solution. Other materials in the cocktail can also absorb the energy from light and re-emit that energy, thereby possibly exciting scintillator molecules and creating false pluses. To reduce these effects, samples are kept cold and dark before measurement. By keeping the

sample cold, the kinetic energy from mechanical mixing is reduced. By keeping the sample dark, fluorescence effects are allowed to cool.

In order to optimize the results from liquid scintillation detectors, the results are characterized by a figure of merit (FOM). The FOM is used to optimize the signal to noise ratio or the ratio between the sample counts and background counts. The FOM is calculated by finding the Region of Interest (ROI) in which this ratio is optimized. The FOM is defined as dividing the efficiency squared (as a percentage) by the background count rate C_b in cpm of the desired ROI as shown in Equation 3.

$$FOM = \varepsilon^2/C_b \quad (3)$$

The application of this FOM will be discussed later.

MATERIALS AND METHODS

Strontium-Specific Extraction Chromatography Resin

Extraction chromatography uses a collection of beads packed into a column to selectively absorb a particular chemical. These beads consist of three main components: the inert support matrix, the stationary phase, and the mobile phase. (Horwitz, 2015) The inert support phase provides a structural support system for the stationary phase much like a sponge. This matrix typically consists of an organic polymer or porous silica ranging in size from 50 to 150 µm in diameter. (Horwitz, 2015) The stationary phase consists of a liquid extractant consisting of a single compound or a mixture. The mobile phase is usually an acid solution. Sometimes, though, complexants (oxalic or hydrofluoric acids) are used to enhance selectivities or the stripping of strongly retained metal ions from columns. (Horwitz, 2015)

The Sr Resin by Eichrom uses 1M 4,4'(5')-di-t-butylcyyclohexano 18-crown-6 (crown ether) in 1-octanol as its extractant. For the chemical composition of this crown ether, see Figure 4: Eichrom's Sr Resin Extractant. Notice the ring of oxygen available for bonding in the center of this molecule. The primary reason this resin works to separate strontium from other ions is the space inside the ring of oxygen molecules. The strontium ion has an effective ionic radius of 118 picometers (pm) and fits just inside this ring of oxygen atoms. This also explains why the resin is selective for lead as well as its effective ionic radius is 119 pm.

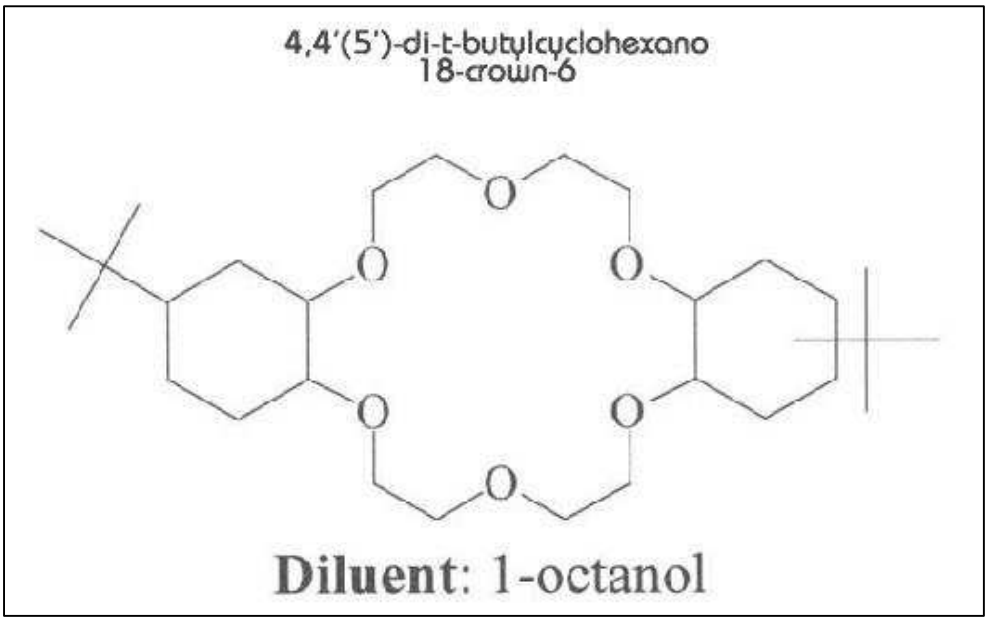

Figure 4: Eichrom's Sr Resin Extractant

Another reason this resin works to separate strontium from other ions is based on acid dependencies of various ions at different acid concentrations. See Figure 5: Acid Dependency of k' for Various Ions at 23-25ºC Sr Resin for the graphical representation of these dependencies. Per these graphs, the ability to absorb strontium (Sr (II)) by the column increases to a maximum at 8 M HNO_3 whereas all other ions decrease significantly.

Another reason these columns work to separate strontium is the ability to elute only strontium once absorbed onto the column. Since "The retention of Pb by Sr Resin is high across a broad range of nitric acid concentrations," (Sr Resin, 2015) the strontium can be eluted from the column while lead remains absorbed. 0.01M HNO_3 is sufficient to elute the strontium. Although water works to elute the strontium from the column, it will also elute the lead. For this reason, the 0.01M HNO_3 is used to selectively elute the strontium.

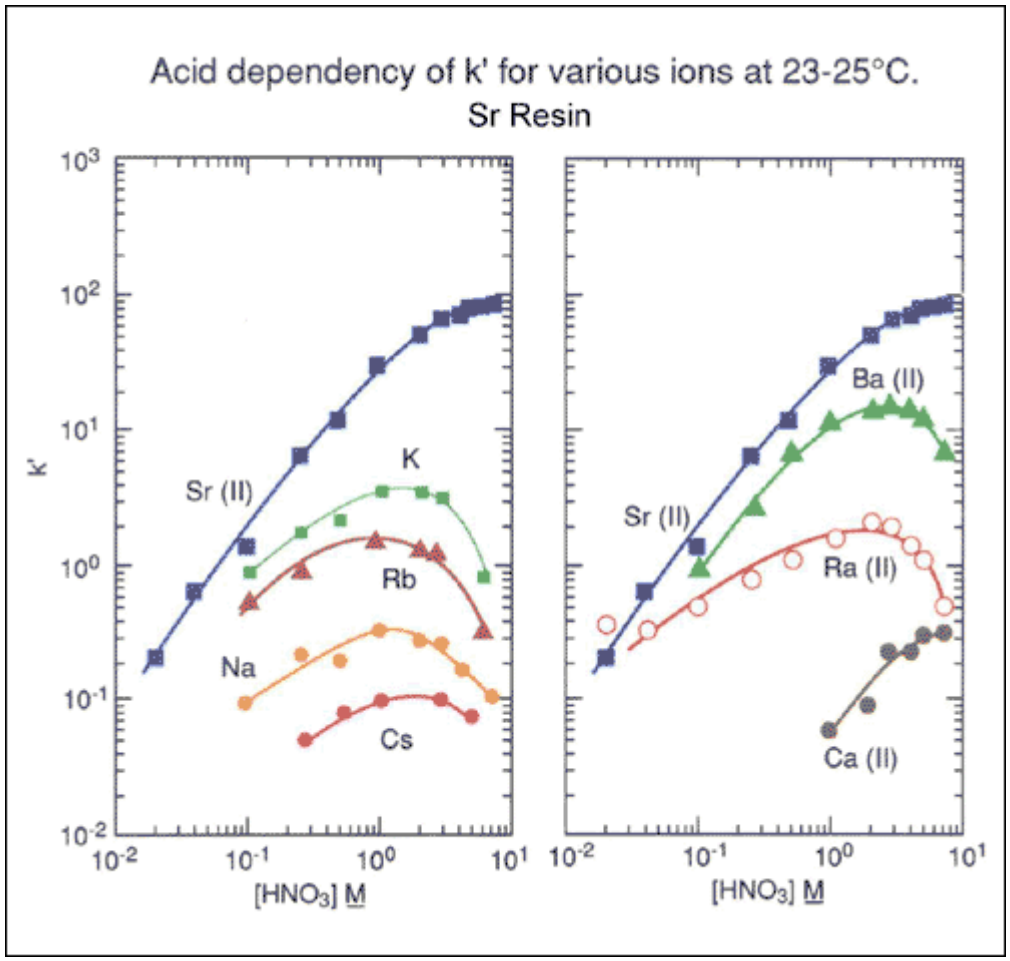

Figure 5: Acid Dependency of k' for Various Ions at 23-25ºC Sr Resin (Sr Resin, 2015)

Experimental Procedure

The overall process used for this study can be divided into the ten separate steps and observations below:

1) Sample Collection
2) Sample Preparation
3) Leaching
4) Filtering
5) Pre-loading
6) Loading
7) Rinsing
8) Elution
9) Concentration and Removal of Excess Acid
10) Measurement
11) General Observations During the Separation Process and Analysis

Sample Collection

The first step in this analysis was to collect vegetation and soil samples from various locations near the Fukushima Nuclear Power Plant. This was accomplished on June 4, 2013 at locations listed in Table 1: Sample Type, Location and Distance from the FDNPP.

Table 1: Sample Type, Location and Distance from the FDNPP

Sample ID		Location (Refer to Appendix for Coordinates)	Distance from Gate (km)
Soil	Vegetation		
F1-19	F2	Gate	0
F1-15	E1	Roadside	1
F1-11	D1	Roadside	1.5
F1-24	G1	Roadside	4.1
F1-09	C1	Chemeiji	8.5
F1-32	H1	Roadside	15
F1-04	B1	Odaka Minamisoma	17.8
F1-01	A1b	Iitate Village	40

Vegetation samples were collected in 6” resealable plastic bags. These bags were each placed inside an additional 6” resealable bag and kept in a cooler filled with ice. A picture of the vegetation samples is shown in Figure 6: Vegetation and Soil Samples. The vegetation samples were representative of the foliage at each sampling location.

The soil samples were taken with a corer that measured 2 1/4” in diameter and 6” in length. A representative picture of the soil samples is shown in Figure 7: Soil Sample (representative). These samples were dissected in 1” intervals for a total of 6 individual 1” layers of 2 1/4” diameter from each core sample. These samples were kept in a cooler filled with ice as well.

Figure 6: Vegetation and Soil Samples

Figure 7: Soil Sample (representative)

Once received at Colorado State University, the soil and vegetation samples were kept in a freezer located in the Environmental Health and Radiological Sciences department until the strontium separation process was conducted in June 2014.

Sample Preparation

To begin, an empty flask was weighed and its mass recorded. A frozen vegetation sample was then placed into the weighed flask. Enough vegetation was used to fill the flask to 1/3 – 1/2 its volume. The flask was then re-weighed and its mass recorded. The flask was then placed into an oven for 48 hours that was set at 58 ^{o}C in order to rid the vegetation of any moisture. The flask was removed from the oven and allowed to cool to room temperature. The flask, now with dry vegetation, was weighed and its mass recorded. By subtracting the weight of the empty flask from the weight of the flask with the dry vegetation, the mass of the vegetation was calculated.

This same sample preparation procedure was followed for the soil samples as well. Instead of filling an empty flask to 1/3 - 1/2 its volume, a 1” cross-section of soil with 2 1/4" diameter was placed in the flask. The upper-most 2” of each soil sample was used from each sampling location (2 samples of 1” depth each). For the remainder of this analysis, both vegetation and soil samples were handled identically unless otherwise noted. The mass of each vegetation and soil sample is shown in the Appendix in Table 5: Sample Type, Location and Mass.

Leaching

The following items were placed into a reflux boiler:

1) One soil or vegetation sample (approximately 5-15 g)
2) 4 mL of 8M nitric acid (HNO_3)
3) 1 mL strontium nitrate ($Sr(NO_3)_2$) carrier (1.2 mg/mL)
4) 1 mL hydrogen peroxide (H_2O_2)
5) 2 mL 16M HNO_3

The solution was kept at 8M HNO_3 and boiled for 60 minutes. At the 30 minute mark, if needed, the additional items were added to the reflux boiler to keep the vegetation from drying out.

1) 4 mL 8M HNO_3
2) 1 mL H_2O_2
3) 1 mL 16 M HNO_3

The hydrogen peroxide was used in combination with 8M nitric acid to best digest the vegetation. The 16M nitric acid was used to keep the overall concentration of the mixture's nitric acid concentration at 8M, i.e., if 1 mL H_2O_2 is added, then 1 mL of 16M HNO_3 was added to bring the entire mixture to 8M nitric acid.

Filtering

Upon completion of boiling for an hour, the sample mixture was poured through a Büchner funnel into a vacuum flask (Figure 8: Vacuum Flask and Büchner Funnel) to separate the aqueous phase from the vegetation/soil. The radionuclides leached from the vegetation/soil

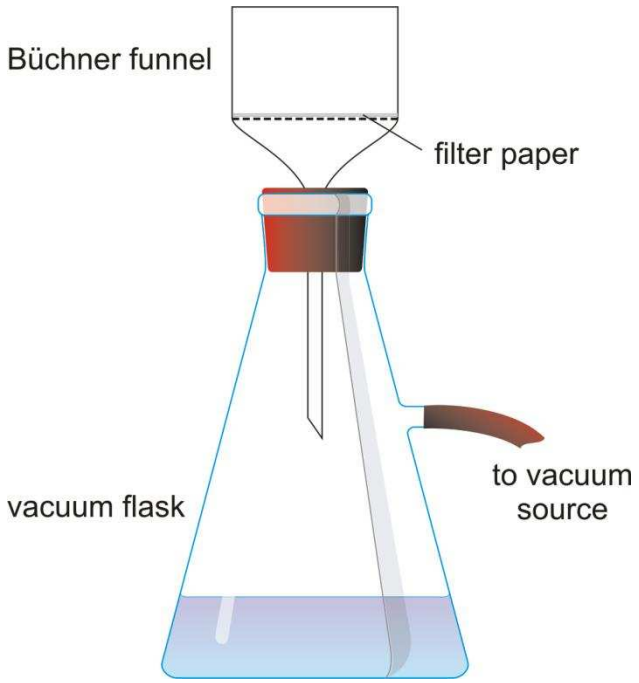

Figure 8: Vacuum Flask and Büchner Funnel (Generalic, 2015)

were carried through the funnel along with the nitric acid. The plant/soil material remained on the filter paper in the funnel.

Six mL of 8M HNO_3 were applied to wash the boiling flask in 1 mL increments, and 10 x 1 mL was applied to wash the vegetation/soil media to ensure the maximum transfer of strontium to the aqueous phase. The vacuum flask was allowed to operate for approximately 10 minutes until the vegetation/soil was visibly dry.

Pre-loading

To prepare for this step, a vacuum box was set up as seen in Figure 9: Vacuum Box Diagram. The vacuum box was operated at 5" Hg vacuum pressure. This amount of vacuum

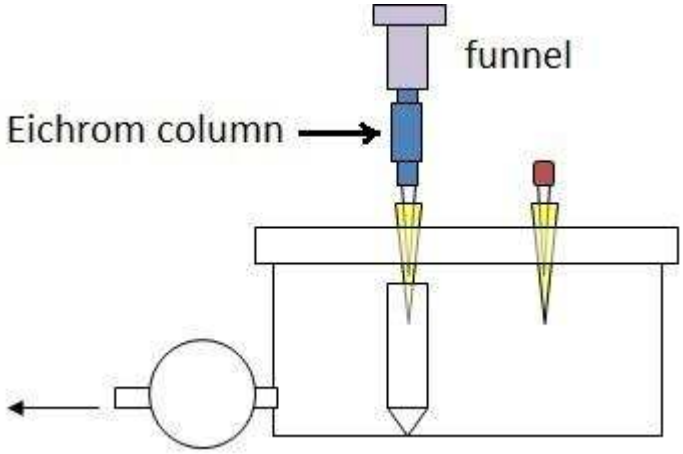

Figure 9: Vacuum Box Diagram

pressure allowed for quicker operation of the column. At higher vacuum pressures, the rate of column transfer was greater than our target of 1 drop per second exiting the column.

In this step, the strontium-selective SR-resin-B columns (100-150 µm) by Eichrom®/Triskem International® were subjected to a rinse using 10 mL of de-ionized water followed by a rinse of 7 mL of 8M HNO_3. This was done to condition the columns for the aqueous mixture per Eichrom instructions.

Loading

The next step of the process was to load the Eichrom column with the aqueous strontium solution from the vacuum flask. This was done by simply pouring the flask contents into the funnel of the vacuum box. Once emptied, the vacuum flask was rinsed with 4 mL of 8M HNO_3 in 1 mL increments to ensure all of the strontium was transferred out of the flask and into the

column. After rinsing the flask, 6 mL of 8M HNO_3 was added to the column in 1 mL increments. The purpose of this step was to absorb the ^{90}Sr onto the column.

Rinsing

Next, 10 mL of a 3M HNO_3/0.05 M oxalic acid mixture was added to the column in 1 mL increments to wash impurities from the column (with the exception of the aforementioned lead). "The tetravalent actinides show significant retention on the Sr Resin. The addition of oxalic acid as a competitive complexing agent will prevent the retention of actinide elements on the column." (Sr Resin, 2015)

Elution

The purpose of this step was to remove the strontium from the column while allowing the absorbed lead to remain in the column. To accomplish this, 10 mL of 0.01M HNO_3 was added to the column in 1 mL increments.

Concentration and Removal of Excess Acid

The purpose of this step was twofold. As the liquid scintillation vials hold approximately 22 mL of liquid, it is important to concentrate the strontium into the smallest liquid volume possible. This would allow for the maximum amount of LSC cocktail to be added to the vial which would aid in detection. The second purpose of this step was to drive off the 0.01 M HNO_3, which could potentially cause inferences with the scintillation cocktail during LSC analysis.

The eluate from the previous step was transferred from a 100 mL vial into a small glass flask. Two boiling stones were then added to the flask. Then the flask was placed on a heat mushroom and placed under a fume hood. As the mixture was boiled, 1 mL of de-ionized water was added as the flask neared emptiness. This was done 10 times for a total addition of 10 mL of de-ionized water, most of which was boiled off in the process.

Upon completion of the boiling, the remaining liquid (~0.03 mL) was pipetted into a liquid scintillation vial. Then 0.5 mL of de-ionized water was pipetted into the empty flask and swirled gently to ensure capture of all the strontium. The liquid was then pipetted from the flask into the LSC vial. This was done four times for a total rinse of 2 mL of de-ionized water.

Measurement

All of the vegetation and soil samples were prepared in the same fashion and placed into a 22 mL vial along with 18 mL of Perkin-Elmer's Ultima Gold™ cocktail. Immediately following the strontium separation process, samples were placed into the rack of the Hidex 300SL LSC. Samples were allowed to dark-correct for six hours. Then, the samples were each measured three times for 6000 seconds during each repeat. The first measurement of each sample was discarded to reduce the influence of kinetic movement of the sample just prior to measurement. The LSC operates by moving the sample to be measured from a staging tray into the detector just prior to measurement. The average of the 2nd two measurements of each sample were used as the average counts of the sample.

Results from the LSC were imported from a comma-separated file (.csv) into the Hidex Microsoft Excel© spreadsheet. Once in the Hidex spreadsheet, the Region of Interest (ROI) was applied to the sample to reduce the influence of background radiation and determine the total number of counts of the strontium.

The ROI was determined by using IAEA Standard 373 Grass with known activity. The first step was to calculate the current activity of the standard.

This was accomplished using the following formula for determining current activity:

$$A = A_o e^{-\lambda t} \quad (4)$$

where:

A = current activity

A_o = initial activity

λ = decay constant

t = time difference from initial to current activity

The IAEA standard was prepared on 1/1/1991 with an initial beta activity of 1320 mBq/g of solution. Using the above formula, we calculated the activity as of 11/21/2014 to be 742.39 mBq/g. Using this activity, the count rate (cpm) was calculated using the following equation:

$$cpm = \left(\frac{A}{1000}60\right)(m)(\varepsilon_p)(2) \quad (5)$$

where:

A = current activity (742.39 mBq/g)

m = mass of the standard sample (0.71g)

ε_p = process extraction efficiency (85%)

2 = represents the ingrowth of ^{90}Y due to secular equilibrium

On the measurement date of 11/21/2014, our standard was determined to have 53.49 cpm.

Using the calculated value of cpm for the IAEA standard, the figure of merit (FOM) was determined using the Hidex spreadsheet with the LSC results of measuring the IAEA standard. The first step in accomplishing this was to subtract the average of eight measurements of background radiation from the average of five measurements of the standard. This produced the actual measurement of the standard as 43.85 cpm. Recalling the FOM equation from earlier:

$$FOM = \varepsilon^2/C_b \quad (3)$$

where:

ε = efficiency (measured cpm/actual cpm (43.85/53.49)

C_b = Background cpm

Inserting the FOM equation into the Hidex spreadsheet, the ROI could be manually manipulated to give the highest value for the FOM. Using an iterative process of changing minimum and maximum values for the ROI, the highest FOM occurred at an ROI range for channel numbers 200 to 818. This ROI was used for analysis of all the Fukushima samples in order to reduce the interference of background radiation on the sample measurements.

Once all of the samples were measured immediately following the separation process, they were allowed to sit for a minimum of 21 days to allow for ingrowth of ^{90}Y. ^{90}Sr decays via beta emission to ^{90}Y which decays via beta emission to stable ^{90}Zr. The half-life of ^{90}Y is 64 hours. Therefore, after approximately 7 * 64 hours (18.67 days), the ^{90}Sr and ^{90}Y have reached secular equilibrium and decay at the same rate. Measurements of the samples after 21 days should have roughly twice the activity of the measurements taken directly following the strontium separation process. Measurement of the samples after 21 days was a good indicator of the presence of ^{90}Sr if the count rate doubled in the second measurement.

In order to quickly gauge the relative efficiency of our separation process, a local vegetation sample and a local soil sample were subjected to the process to act as blanks. Then, a local vegetation sample and a local soil sample were spiked with a known amount of ^{85}Sr and subjected to the separation process. This sample was analyzed on the HPGe detector as ^{85}Sr emits discrete gamma photons at 514 keV (amongst others). This allows for quick and easy detection and quantification of ^{85}Sr. The percentage yield from our process using the HPGe was found to be 80%. This information was used to benchmark the separation process to determine a

rough estimate of its effectiveness. Further definition of our process efficiency using the LSC was calculated with the IAEA ^{90}Sr standard that was subjected to the separation process.

To further define the actual yield of the process, a vegetation blank and soil blank were spiked with the IAEA standard of known activity. This is different than discussed in the FOM section above as the standard was subjected to the entire separation process as opposed to only being measured in order to determine the ROI. Results of the yield for the separation process were determined to be 85% for the vegetation samples and 88% for the soil samples. These values were used in the final evaluation of the activity of the samples. All samples were time corrected to display their activity on the sampling date of 6/4/2013.

General Observations During the Separation Process and Analysis

A couple of interesting observations occurred during the analysis of the samples. The first of these is the cloudiness of some of the samples following the separation process. This clouding of the sample rendered it unmeasurable by the LSC due to quench. During the initial development of the process, no de-ionized water was added during the concentration phase of the process. The sample was originally boiled long enough to reduce the aqueous content and then transferred to the LSC vial. A few of these samples became cloudy when the Ultima Gold™ was added to the vial. The addition of de-ionized water during the concentration phase was developed to try to combat this condition and seemed to work at first. Mid-way through the samples, new flasks were introduced to the process. These flasks were made such that the neck of the flask contained much more glass than the original flasks. It was noted during the concentration phase of the process that the new flasks tended to condense water on the inside of their necks while boiling. This was noticed on the first use of the new flasks. Ultimately, the concentrated sample became cloudy upon addition of the Ultima Gold™ cocktail even though de-ionized water was used during the concentration phase. To combat this, a Bunsen burner was

used during the concentration phase to keep the neck of the flask heated to prevent condensation. This change was instituted about half way through our separation of the samples. Using this method, none of the remaining samples became cloudy upon addition of the Ultima Gold™ cocktail. This cloudiness is a known issue with the scintillation cocktail when using high-molarity nitric acid. When using nitric acid of 5M or higher molarity, the nitric acid dissociates and releases nitrogen dioxide (a brown gas) which can cloud the mixture. (Perkin Elmer, 2007)

A second observation noted during our analysis occurred between the time of the initial strontium measurement and the yttrium ingrowth measurement. An unexpected peak appeared in the yttrium spectrum. See Figure 10: ^{90}Y Ingrowth Measurement to view this peak. Conversely, a later measurement of the samples shows the disappearance of this peak in Figure 11: Re-measurement of the After 90Y Ingrowth Re-measurement. The line with the highest

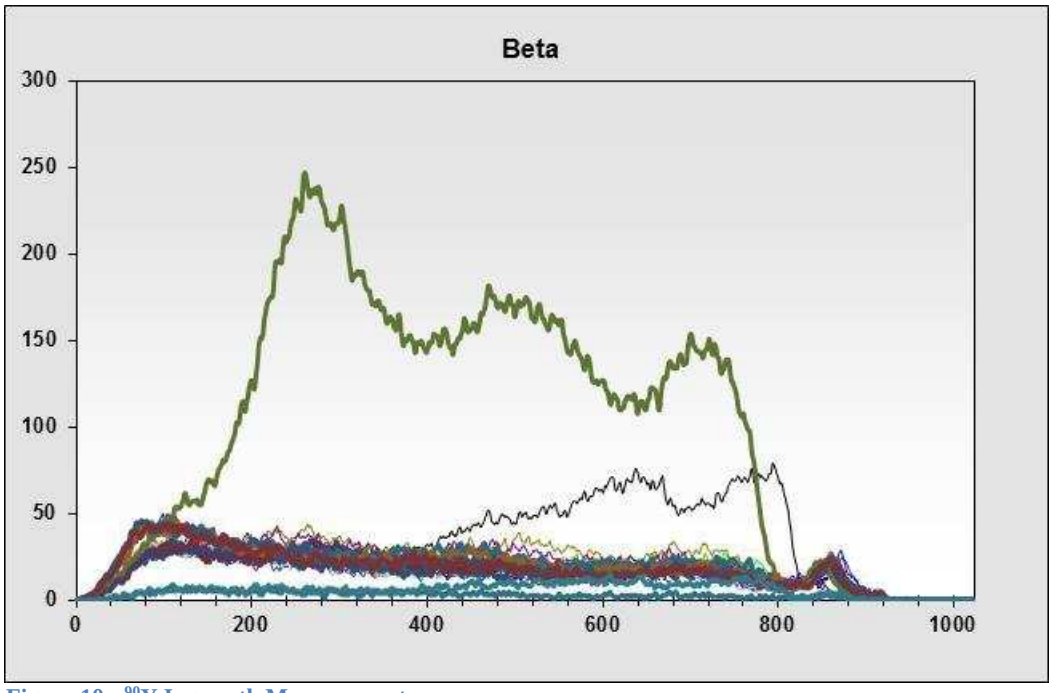

Figure 10: ^{90}Y Ingrowth Measurement
The channel of the LSC is displayed on the abscissa. The number of counts are displayed on the ordinate.

number of counts (green) is the soil sample taken at the gate of Fukushima. The line with the 2nd highest number of counts (black) is the IAEA standard. The appearance of these two lines should be very similar in shape. The soil sample has a peak on the left side of the graph whereas the standard does not. There are multiple potential causes for this peak. The first potential cause is that there is a short-lived radionuclide in the sample. Short-lived because in re-analyzing the samples in April 2015, the peak is no longer there. This is unlikely as the sample had undergone a selective separation for strontium and been in storage for roughly 12 months prior to analysis. A more likely potential cause is mechanical issues with the LSC. In between the initial strontium measurements and the yttrium measurements, the LSC experienced technical difficulties and required maintenance by the manufacturer. Finally, another potential cause is

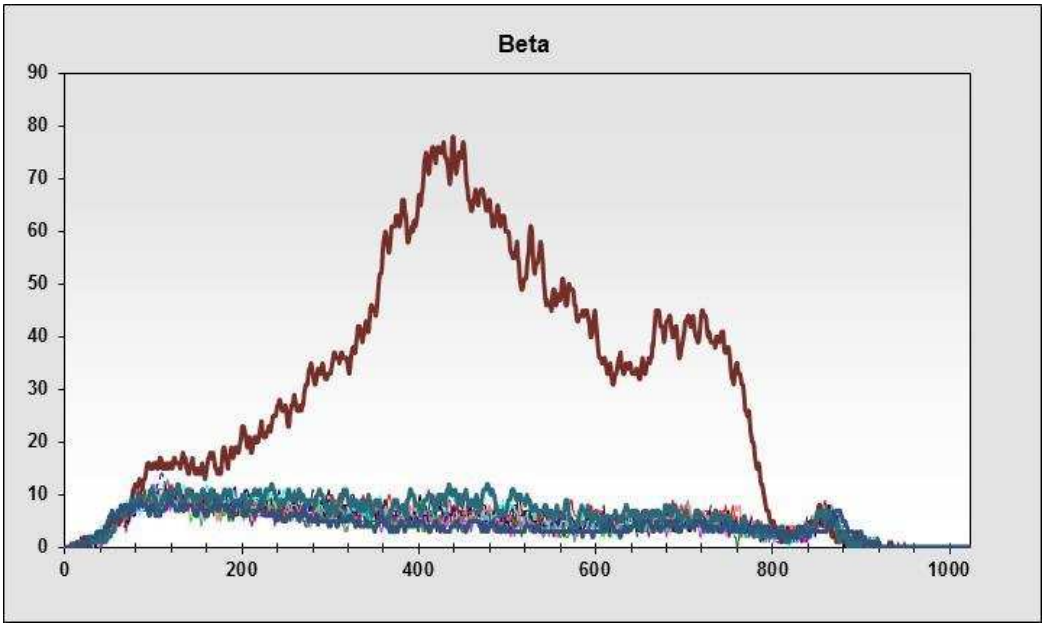

Figure 11: ^{90}Y Ingrowth Re-measurement
The channel of the LSC is displayed on the abscissa. The number of counts are displayed on the ordinate.

due to some sort of chemical interaction of the sample, the Ultima Gold™ cocktail, and/or the LSC vial. Determination of the cause for this mystery peak falls outside of this analysis and would be a good area for further investigation.

Presence of Radioactivity

In order to determine if excess radiation above background radiation exists in a sample, two parameters of the detector must be determined: the decision threshold (y*) and the lower limit of detection (LLD). Two types of error can be found when using a detector: false positives (α) or false negatives (β). To determine the decision threshold, the false positive error is set at 5% and the false negative is set at 50%. After these error levels are set, any amount of counts above this limit is considered excess radioactivity. The decision threshold is used for investigation of radioactivity in the sample. The following equation is used to determine the decision threshold:

$$y^* = 2.33\sqrt{(C_b)} \quad (6)$$

where C_b = background count

The lower limit of detection is used for regulatory purposes and data reporting. This value is found by setting the false positive and false negative probability of occurrence to 5%. The following equation is used to find the LLD:

$$LLD = 2.71+4.65\sqrt{(C_b)} \quad (7)$$

The assumption when using the lower limit of detection and the decision threshold is that the sample and background counting times are equal.

RESULTS AND DISCUSSION

To calculate the activity in Table 2: ^{90}Sr Soil Sample Results and Table 3: ^{90}Sr Vegetation Sample Results, the following equation was used:

$$A = \left(\frac{cpm}{TDCR*60*process\ efficiency*0.5*0.965}\right) \quad (8)$$

where:

A = activity of the sample

cpm = counts per minute

TDCR = triple to double coincidence ratio

process efficiency = 85% for vegetation, 88% for soil

0.5 = correction factor for yttrium-90 ingrowth

0.965 = time correction of activity for time between sampling and measurement

To calculate the specific activity, the activity was divided by the sample mass.

The decision threshold for detection in the LSC was calculated for both the soil and vegetation samples using equation 6:

$$y^* = 2.33\sqrt{(C_b)} \quad (6)$$

The decision threshold for soil and vegetation were 14.78 cpm and 14.54 cpm respectively. Comparison of the sampling results to the decision threshold determined if the sample contained excess radioactivity above background.

The lower limit of detection for the LSC was calculated for both the soil and vegetation samples using equation 7:

$$LLD = 2.71+4.65\sqrt{(C_b)} \quad (7)$$

The LLD for soil and vegetation was 32.21 cpm and 31.73 cpm respectively. The LLD was met for every sample analyzed. This confirms the LSC was able to detect any ^{90}Sr present in the samples.

Table 2: ^{90}Sr Soil Sample Results

Sample ID	Average (cpm)	Standard Deviation (cpm)	Lower Limit (cpm)	Upper Limit (cpm)	Excess Radio-activity?	Activity (Bq)	Activity Concentration (Bq/kg)
F1-01-T1	13.08	1.05	12.03	14.13	n	0.1601	17.09
F1-01-T2	7.51	0.27	7.24	7.78	n	0.0947	10.95
F1-04-T1	5.005	0.84	4.16	5.85	n	0.0637	5.64
F1-04-T2	5.095	0.30	4.79	5.40	n	0.0663	10.78
F1-09-T1	6.95	0.42	6.53	7.37	n	0.0878	8.93
F1-09-T2	5.255	1.11	4.14	6.37	n	0.0676	7.66
F1-11-T1	16.86	0.52	16.34	17.38	y	0.2038	86.45
F1-11-T2	9.695	0.87	8.83	10.56	n	0.1209	16.72
F1-15-T1	11.53	0.82	10.71	12.35	n	0.1440	9.08
F1-15-T2	13.93	0.88	13.05	14.81	m	0.1734	11.37
F1-19-T1	248.12	1.43	246.69	249.55	y	2.5670	385.27
F1-19-T2	20.4	0.82	19.58	21.22	y	0.2458	28.67
F1-24-T1	20	0.24	19.76	20.24	y	0.2395	12.88
F1-24-T2	14.295	0.84	13.45	15.14	m	0.1749	14.18
F1-32-T1	9.81	1.54	8.27	11.35	n	0.1225	12.58
F1-32-T2	8.835	1.44	7.40	10.27	n	0.1107	9.11

CPM = counts per minute TDCR = triple to double coincidence ratio Activity as of 6/4/2013

Table 3: ^{90}Sr Vegetation Sample Results

Sample ID	Average (cpm)	Standard Deviation (cpm)	Lower Limit (cpm)	Upper Limit (cpm)	Excess Radio-activity?	Activity (Bq)	Activity Concentration (Bq/kg)
Veg A1b	2.805	0.11	2.70	2.91	n	0.0381	30.33
Veg B1	9.325	2.21	7.11	11.54	n	0.1269	21.13
Veg C1	7.755	0.12	7.63	7.88	n	0.1024	49.13
Veg D1	22.14	0.06	22.08	22.20	y	0.2767	56.12
Veg E1	28.775	0.54	28.23	29.32	y	0.3464	147.77
Veg F2	21.555	1.53	20.02	23.09	y	0.2626	59.83
Veg G1	16.605	0.28	16.33	16.88	y	0.2197	16.43
Veg H1	2.495	0.84	1.65	3.34	n	0.0331	10.28

CPM = counts per minute TDCR = triple to double coincidence ratio Activity as of 6/4/2013

Soil Results

As seen in Table 2: ^{90}Sr Soil Sample Results, ^{90}Sr was found with 95% confidence in four of the soil samples based on the exceedance of the decision threshold. Two other samples could potentially contain ^{90}Sr due to the upper limit exceeding the decision threshold. These two samples had a lower limit below the decision threshold; however, so the presence of ^{90}Sr in these samples cannot be confirmed. The four soil samples that were positive for the presence of ^{90}Sr were located within 4.1 km of the FDNPP gate. The highest concentration at 385.27 Bq/kg was found at the FDNPP gate in the uppermost 1" of soil.

For comparison, the activity of a few radionuclides were calculated using Taylor's et al concentration of elements in the earth's upper crust. (Taylor, 1985) The following equation was used to calculate these activities:

$$A = \lambda N \tag{9}$$

where:

λ = decay constant

N = number of atoms

To find the number of atoms (N) the following equation was used:

$$N = (soil\ concentration)(natural\ abundance)\left(\frac{g}{1000\ mg}\right)\left(\frac{1}{mw}\right)(Avogadro's\ \#) \tag{10}$$

where:

soil concentration = in mg/kg (Taylor, 1985)

natural abundance = ratio of naturally occurring radioactive nuclide (Magill, 2012)

mw = molecular weight of the radionuclide

Avagadro's # = 6.02×10^{23} atoms/mol

See Table 4: Comparison of the Average Abundance of Naturally Occurring Radionuclide Activities vs. Strontium-90 from FDNPP for the results of these calculations. The average

concentration of radionuclides in the upper crust is taken from Taylor's et al. *The Continental Crust: Its Composition and Evolution* (1985) and the abundance is taken from Magill's et al.

Table 4: Comparison of the Average Abundance of Naturally Occurring Radionuclide Activities vs. Strontium-90 from FDNPP
(Taylor, 1985), (Magill, 2012)

Radionuclide	Concentration (mg/Kg)	Abundance	Molecular Weight (g/mol)	Activity (Bq/Kg)
Uranium - 238	2.8	99.270%	238	40.33
Thorium - 232	10.7	100%	232	47.44
Potassium - 40	28000	0.012%	40	101,014
Strontium - 90	0	0.000%	40	385*
* Determined experimentally in this project				

Chart of the Nuclides, 8th Edition (2012). These two values were used in equations 9 & 10 to calculate the naturally occurring activity concentration of these radionuclides in the environment. This comparison, of course, does not imply ultimate radiological comparability of these radionuclides, as their decay modes and metabolic properties are clearly distinct. However, using these numbers allows for a rough comparison of measured anthropogenic radionuclides with the average activity range of natural radioactivity. As seen in the table, the experimentally determined activity of ^{90}Sr found at the gate of FDNPP was greater than that of naturally occurring uranium-238 and thorium-232 by roughly an order of magnitude, but less than potassium-40. Since ^{90}Sr does not occur naturally, all of its activity is anthropogenic and deposited via nuclear weapon detonations or nuclear power plant releases. Since the highest activity concentrations of ^{90}Sr were found closest to the FDNPP and the samples > 4.1 km away from the FDNPP did not show any radioactivity, it is most likely all of the ^{90}Sr deposited in this area of Japan is a result of the FDNPP accident and not indicative of nuclear weapon detonations.

An interesting observation is that no ^{90}Sr was found at the location 1 km from the gate, but was found 1.5 km from the gate. A couple of ideas could explain this. The first of these is that the cardinal direction of the 1.5 km location is slightly different than those of the other locations where ^{90}Sr was found. All four samples containing ^{90}Sr were either at the FDNPP gate or south-southwest of the gate. The 1.5 km location was southwest of the gate. This implies that the weather during the release of radionuclides from the FDNPP could have played a role in their deposition. Another potential explanation is the difference of geography/geology. Since the soil samples were not subjected to an analysis of soil type and their geological data were not recorded, it is possible that one or both of these factors had an influence on the deposition and/or retention of the ^{90}Sr. Further investigation into these ideas could potentially lead to a better understanding of why ^{90}Sr was found at various distances and directions from the FDNPP.

Vegetation Results

As seen in Table 3: ^{90}Sr Vegetation Sample Results, ^{90}Sr was found with 95% confidence in four of the vegetation samples based on the exceedance of the decision threshold. The four vegetation samples that were positive for the presence of ^{90}Sr were located within 4.1 km of the FDNPP gate. The highest concentration of 147.8 Bq/kg was found at 1 km from the FDNPP gate. This is different from the maximum activity concentration found in the soil (1 km for vegetation vs. 0 km for soil). The determination of why this occurred is outside the scope of this project and could potentially be an area of further investigation.

Also unlike the soil samples, there were no vegetation samples that could possibly be positive for excess radiation without confirmation.

Finally, the vegetation sample at 1 km was confirmed to have ^{90}Sr whereas the soil sample at 1 km could not be confirmed as having ^{90}Sr.

CONCLUSIONS

A couple of conclusions can be made concerning this study. The first of these is the existence of ^{90}Sr in 8 samples (4 vegetation, 4 soil) within 4.1 km of the FDNPP with 95% confidence. A few of these samples contained a higher activity concentration of ^{90}Sr (soil maximum = 385 Bq/kg, vegetation maximum = 148 Bq/kg) than a couple of naturally occurring radionuclides (^{238}U and ^{232}Th) and less activity concentration than ^{40}K.

Although activity concentrations of ^{90}Sr at the upper limits were an order of magnitude greater than naturally occurring ^{238}U and ^{232}U, the levels do not pose a significant health threat to individuals based on the following reasoning. Humans do not typically ingest soil, so this reasoning focuses on the vegetation sample results. According to *Radioactivity and Radiation Limits and Benchmarks*, Table 5.c., the safe limit of ingestion for a primary food product is 750 Bq/kg for ^{90}Sr. (Association for Radiation Protection, 2003) Assuming the vegetation sample with the highest activity concentration of 147.77 Bq/kg is lettuce or rice, ingestion of this is 20% of the recommended safe limit of 750 Bq/kg if it were consumed as a primary food source.

Secondly, the separation process using the SR-resin-B columns (100-150 µm) by Eichrom®/Triskem International® to leach ^{90}Sr from vegetation and soil and subsequently analysis using the Hidex 300SL LSC is an effective method; however it is time-consuming and laborious. Each sample took approximately 36+ h from sample preparation through analysis. Yield results were 85% for the vegetation and 88% for the soil.

REFERENCES

Aoyama, M. H. (2004). Artificial Radionuclides Database in the Pacific Ocean: HAM Database. *The Scientific World Journal*, 200-216.

Association for Radiation Protection. (2003). *Radioactivity and Radiation Limits and Benchmarks.* Germany: A New.

Ball, J. B. (2014). Liquid Scintillation Detectors. *ERHS 531: Nuclear Instruments and Measurements*. Colorado State University.

Cember, H., & Johnson, T. E. (2009). *Introduction to Health Physics, Fourth Edition.* New York: McGraw Hill.

Generalic, E. (2015, February 22). *Buchner Funnel*. Retrieved June 25, 2015, from Chemistry Glossary: http://glossary.periodni.com/dictionary.php?en=Buchner+funnel

Horwitz, E. P. (2015). *Extraction Chromatography of Actinides and Selected Fission Products: Principles and Achievement of Selectivity*. Retrieved June 23, 2015, from www.eichrom.com: www.eichrom.com/eichrom/products/extraction.aspx

Kinoshita, N. S. (2011 Vol 108 No 149). Assessment of Individual Radionuclide Distributions from the Fukushima Nuclear Accident Covering Central-East Japan. *Proceedings of the National Academy of Sciences of the United States of America*, 19526-19529.

Kirchner, G. B. (2012). Radioactivity from Fukushima Dai-ichi in Air Over Europe; part 2: What Can it Tell Us About the Accident? *Journal of Environmental Radioactivity*, 23-34.

Kiyoshi, K. (1964). Radioactive Contamination of Rice in Japan with Reference to Sr-90 and Cs-137 Content in Rice Until 1962. *Journal of Radiation Research*, 116-119.

Kocadag, M. M. (2013 Volume 28, No. 2). On the Interference of 210Pb in the Determination of 90Sr Using a Strontium Specific Resin. *Nuclear Technology & Radiation Protection*, 163-168.

Lipscy, P. K. (2013). The Fukushima Disaster and Japan's Nuclear Plant Vulnerability in Comparative Perspective. *Environmental Science and Technology*, 6082-6088.

Madigan, D. B. (2012 vol 109 no 24). Pacific Bluefin Tuna Transport Fukushima-derived Radionuclides from Japan to California. *Proceedings of the National Academy of Sciences of the United States of America*, 9483-9486.

Magill, J. P. (2012). Chart of the Nuclides, 8th Edition 2012. In J. P. Magill, *Karlsruher Nuklidkarte* (p. 52). Germany: Nucleonica GmbH.

McKenna, T. J., & Glitter, J. G. (1988). *Source Term Estimation During Incident Response to Severe Nuclear Power Plant Accidents.* Washington, DC: U.S. Nuclear Regulatory Commission.

Merz, S. S. (2012). Anthropogenic Radionuclides in Japanes Food: Environmental and Legal Implications. *Environmental Science and Technology*, 1248-1256.

Merz, S. S. (2015). Analysis of Japanes Radionuclide Monitoring Data of Food Before and After the Fukushima Nuclear Accident. *Environmental Science and Technology*, 2875-2885.

Nuclear Fission Yield. (n.d.). Retrieved June 25, 2015, from University of Waterloo: www.science.uwaterloo.ca/~cchieh/cact/nuctek/fissionyield.html

Parsons, J. (Spring 2014). *ERHS 531 Lab Handout, Laboratory 3: Counting Statistics.*

Perkin Elmer, I. (2007). *LSC in Practice: Yellowing of Cocktail Mixture Containing Soil Extract.*

Povinec, P. H. (2012). Radiostrontium in the Western North Pacific: Characteristics, Behavior, and the Fukushima Impact. *Environmental Science and Technology*, 10356-10363.

Schwantes, M. O. (2012 Volume 46). Analysis of a Nuclear Accident: Fission and Activation Product Releases from the Fukushima Daiichi Nuclear Facility as Remote Indicators of Source Identification, Extent of Release, and State of Damaged Spent Nuclear Fuel. *Environmental Science and Technology*, 8621-8627.

Shozugawa, K. N. (2012 Vol 163). Deposition of Fission and Activation Products After the Fukushima Dai-ichi Nuclear Power Plant Accident. *Enviornmental Pollution*, 243-247.

Sr Resin. (2015). Retrieved from Eichrom.com: http://www.eichrom.com/products/info/sr_resin.aspx

Steinhauser, G. (2014, April 9). Fukushima's Forgotten Radionuclides: A Review of the Understudied Radioactive Emissions. *Environmental Science and Technology*, 4649-4663.

Steinhauser, G. B. (2014). Comparison of the Chernobyl and Fukushima Nuclear Accidents: A Review of the Enviornmental Impacts. *Science of the Total Environment*, 800-817.

Steinhauser, G. M. (2013 Volume 20, Issue 4). Artificial Radioactivity in Environmental Media (air, rainwater, soil, vegetation) in Austria after the Fukushima Nuclear Accident. *Environmental Science and Pollution Research*, 2527-2534.

Steinhauser, G. S. (2013). Concentration of Strontium-90 at Selected Hot Spots in Japan. *PLOS One*, e57760.

Taylor, S. R. (1985). *The Continental Crust: Its Composition and Evolution.* Oxford, London, Edinburgh, Boston, Palo Alto, Melbourne: Blackwell Scientific.

Thielen, H. (2012). The Fukushima Nuclear Accident - An Overview. *Health Physics*, 169-174.

APPENDIX

Table 5: Sample Type, Location and Mass

Sample ID	Location (distance (km) from FDNPP gate and direction)	GPS Coordinates of Sample	Soil or Vegetation Sample	Empty Flask Mass (g)	Flask Mass w/dry Contents (g)	Sample Mass (g)
Veg A1b	Iitate Village (40 NW)	37.61270°N 140.74905°E	Vegetation	*	*	1.257
Veg B1	Odaka Minamisoma (17.8 N)	37.56556°N 140.99194°E	Vegetation	111.07	117.08	6.01
Veg C1	Chemeiji (8.5 N)	37.49556°N 141.00139°E	Vegetation	169.02	171.1	2.08
Veg D1	Roadside (1.5 SSW)	37.41742°N 141.01012°E	Vegetation	88.32	93.25	4.93
Veg E1	Roadside (1 SW)	37.41770°N 141.01510°E	Vegetation	108.72	113.11	4.39
Veg F2	FDNPP Gate (0)	37.41736°N 141.02329°E	Vegetation	110.86	113.2	2.34
Veg G1	Roadside (4.1 SSW)	37.38854°N 141.00825°E	Vegetation	107.84	121.21	13.37
Veg H1	Roadside (15 SSW)	37.31470°N 141.01325°E	Vegetation	93.84	97.06	3.22
F1-01-T1	Iitate Village (40 NW)	37.61270°N 140.74905°E	Soil	111.09	120.46	9.37
F1-01-T2	Iitate Village (40 NW)	37.61270°N 140.74905°E	Soil	93.08	101.73	8.65
F1-04-T1	Odaka Minamisoma (17.8 N)	37.56556°N 140.99194°E	Soil	108.71	120.01	11.3
F1-04-T2	Odaka Minamisoma (17.8 N)	37.56556°N 140.99194°E	Soil	110.85	117	6.15
F1-09-T1	Chemeiji (8.5 N)	37.49556°N 141.00139°E	Soil	169.02	178.85	9.83
F1-09-T2	Chemeiji (8.5 N)	37.49556°N 141.00139°E	Soil	166.04	174.86	8.82
F1-11-T1	Roadside (1.5 SSW)	37.41742°N 141.01012°E	Soil	186.12	188.47	2.35
F1-11-T2	Roadside (1.5 SSW)	37.41742°N 141.01012°E	Soil	171.07	178.3	7.23
F1-15-T1	Roadside (1 SW)	37.41770°N 141.01510°E	Soil	93.08	108.94	15.86
F1-15-T2	Roadside (1 SW)	37.41770°N 141.01510°E	Soil	111.09	126.33	15.24
F1-19-T1	FDNPP Gate (0)	37.41736°N 141.02329°E	Soil	108.72	115.38	6.66
F1-19-T2	FDNPP Gate (0)	37.41736°N 141.02329°E	Soil	93.84	102.41	8.57
F1-24-T1	Roadside (4.1 SSW)	37.38854°N 141.00825°E	Soil	110.86	129.46	18.6
F1-24-T2	Roadside (4.1 SSW)	37.38854°N 141.00825°E	Soil	166.04	178.37	12.33
F1-32-T1	Roadside (15 SSW)	37.31470°N 141.01325°E	Soil	19.02	178.76	9.74
F1-32-T2	Roadside (15 SSW)	37.31470°N 141.01325°E	Soil	101.82	113.97	12.15